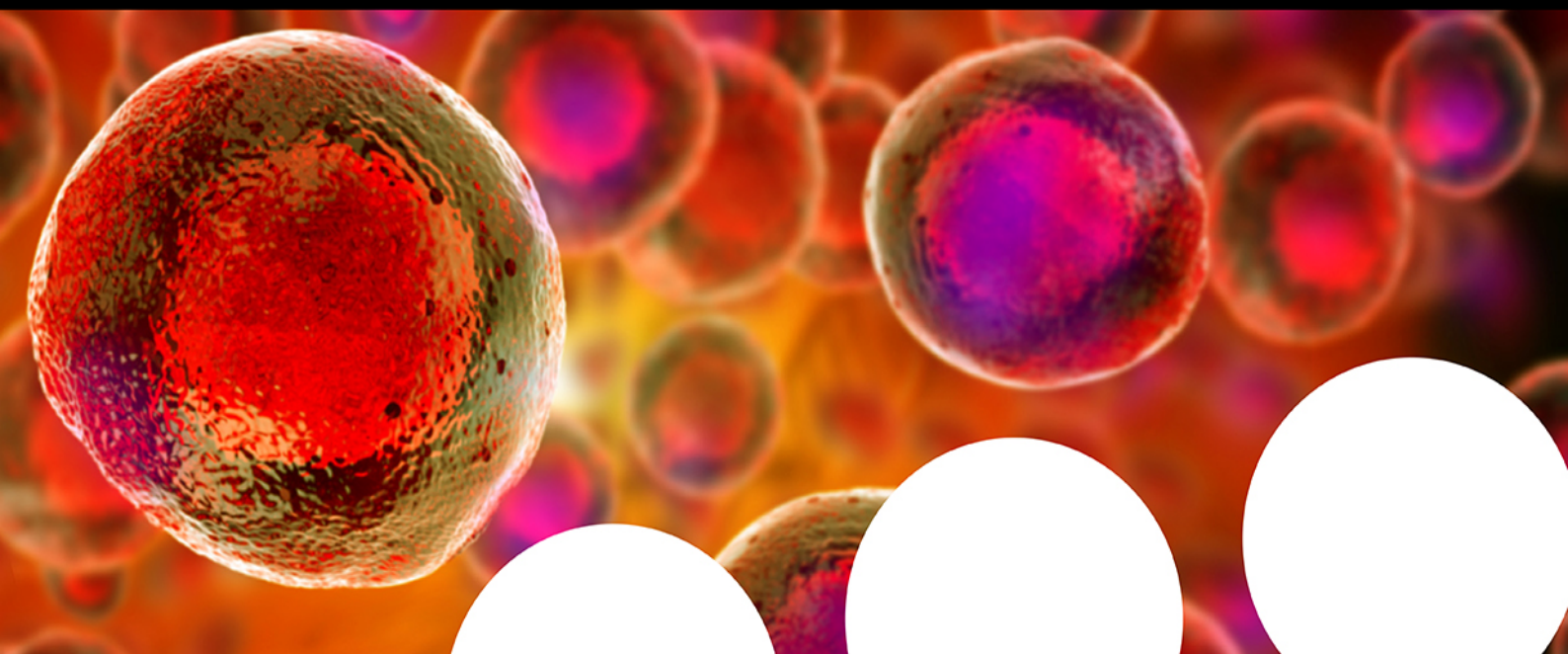


Your research is important and needs to be shared with the world



Benefit from the Chemistry Europe Open Access Advantage

- Articles published open access have higher readership
- Articles are cited more often than comparable subscription-based articles
- All articles freely available to read, download and share.

Submit your paper today.



www.chemistry-europe.org

Formation of a CdO Layer on CdS/ZnO Nanorod Arrays to Enhance their Photoelectrochemical Performance

Thanh Khue Van, Long Quoc Pham, Do Yoon Kim, Jin You Zheng, Dokyoung Kim, Amol U. Pawar, and Young Soo Kang^{*[a]}

The performance and photocatalytic activity of the well-known CdS/ZnO nanorod array system were improved significantly by the layer-by-layer heterojunction structure fabrication of a transparent conductive oxide (TCO) CdO layer on the CdS/ZnO nanorods. Accordingly, a CdO layer with a thickness of approximately 5–10 nm can be formed that surrounds the CdS/ZnO nanorod arrays after annealing at 500 °C under air. At an external potential of 0.0 V vs. Ag/AgCl, the CdO/CdS/ZnO nanorod array electrodes exhibit an increased incident photon to conversion efficiency, which is significantly higher than that of the CdS/ZnO nanorod array electrodes. The high charge

separation between the electrons and holes at the interfaces of the heterojunction structure results from the specific band energy structure of the photoanode materials, and the unique high conductivity of the CdO layer is attributed to the suppression of electron–hole recombination; this suppression enhances the photocurrent density of the CdO/CdS/ZnO nanorod arrays. The photoresponse of the electrodes in an electrolytic solution without sacrificial agents indicated that the CdO layer also has the ability to suppress the well-known photocorrosive behavior of CdS/ZnO nanorods.

Introduction

Among the various types of photocatalytic semiconductor materials, metal oxides, such as TiO₂ ($E_g = 3.2$ eV), ZnO ($E_g = 3.2$ eV), and WO₃ ($E_g = 2.8$ eV), have been studied widely because of the high photocatalytic activity of the surface, long diffusion length, and facile synthetic routes.^[1] In recent years, ZnO nanorod arrays have attracted considerable attention from researchers and are known as a promising material for many applications because of the unique one-dimensionality of these arrays. Single-crystalline nanorods with high surface areas and electrical pathways aligned vertically could be advantageous for efficient electron transport. Therefore, it may be possible to achieve both the strong absorption of photons and efficient charge transport with thicker film devices.^[2] Additionally, ZnO nanorod arrays, which can be synthesized and reproduced easily, can be fabricated on a large scale.^[3] However, the main disadvantage of this material is the wide band gap, which limits the absorption and use of the visible region. To generate electron–hole pairs in the visible region, a narrow-band-gap-sensitizing material should be composited with the ZnO nanorod arrays.^[4] As one of the most important II–VI semi-

conductors, CdS ($E_g = 2.42$ eV) is studied the most widely in different approaches to modify large-band-gap semiconductors. Many studies have been reported on the growth of CdS on ZnO nanorod arrays and the enhancement of the photocatalytic activity because of two important reasons. First, these systems can utilize visible light with narrow-band-gap semiconductors^[5] to result in excellent solar light harvesting. Second, charge transfer from one semiconductor crystal to another can enhance charge separation efficiently by suppressing electron–hole recombination.^[6]


Problems with the growth of CdS on ZnO nanorod arrays are that charge transfer is only effective at the active interface and electron–hole recombination increases as the thickness of the film increases, which thus decreases the photoactivity. To solve this problem, in this study, we reported a simple method to enhance the photoelectrochemical (PEC) properties of CdS/ZnO nanorod arrays by modifying the surface of the CdS layer with a thin layer of CdO. As a semiconductor and transparent conducting oxide (TCO),^[7] the covering layer of CdO is able to enhance the photochemical activity of the CdS/ZnO photoelectrode compared with that of the CdS/ZnO nanorod arrays. The mechanism is discussed further in this paper. The CdO layer somehow protects partially against the well-known photocorrosion of CdS and ZnO materials.

Results and Discussion

From AFM analysis (Figure S1), the average roughness (S_a) and root mean square roughness (S_q) values indicate that the morphology of the surface of the ZnO nanoseed film is similar to the morphology of the ITO surface. The smoothness of the

[a] T. K. Van,⁺ L. Q. Pham,⁺ D. Y. Kim, J. Y. Zheng, D. Kim, A. U. Pawar, Prof. Y. S. Kang
Korea Center for Artificial Photosynthesis
Department of Chemistry
Sogang University
Seoul (Korea)
Fax: (+82) 2-701-0967
E-mail: yskang@sogang.ac.kr

[⁺] These authors contributed equally to this work.

 Supporting Information for this article is available on the WWW under <http://dx.doi.org/10.1002/cssc.201402365>.

ZnO nanoseed film is one of the factors required to obtain highly aligned ZnO nanorod arrays. SEM images of the top and cross-sectional views of the ZnO nanorod arrays for different concentrations of the equimolar reaction solution of $\text{Zn}(\text{NO}_3)_2$ and hexamethylenetetramine (HA) are shown in Figure S2. The length and diameter of the ZnO nanorods increase with an increasing concentration of $\text{Zn}(\text{NO}_3)_2$. For a $\text{Zn}(\text{NO}_3)_2$ concentration of 0.05 M, we obtain arrays of ZnO nanorods with diameters of approximately 100 nm and lengths of approximately 2.5 μm . For a precursor concentration of 0.1 M, these values are 150 nm and 3.0 μm , respectively. The gradual increase of temperature also results in the slow growth of the ZnO nanorods. In addition, the ZnO nanorod array density also increases if the concentration of the precursors increases. Consequently, a thin film of the ZnO nanorod arrays with controlled length, diameter, and density could be obtained easily. The cross-sectional SEM images shown in Figure S2 illustrate that at an equimolar precursor concentration of 0.1 M, the density of the ZnO nanorods is too high to leave spaces between the rods. The film is almost compact. The subsequent step of CdS deposition might be difficult. We optimized the concentration of equimolar precursors at 0.075 M to obtain arrays of ZnO nanorods with diameters of 150–200 nm and lengths of 3.0 μm ; these arrays are suitable for the subsequent deposition of the CdS layer and are used for further steps. A typical TEM image and the corresponding selected area electron diffraction (SAED) pattern (inset) of a ZnO nanorod are shown in Figure 1c. The SAED pattern reveals that the ZnO nanorod is single crystalline.

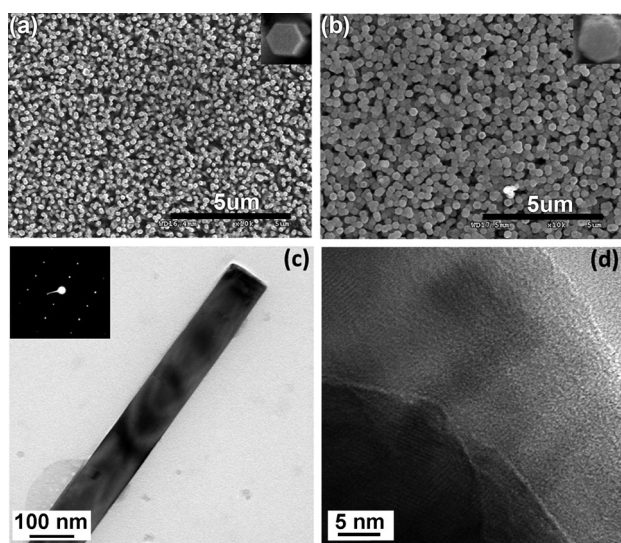


Figure 1. SEM images (top view) of (a) ZnO nanorod arrays and (b) CdS/ZnO nanorod arrays. TEM images of (c) ZnO nanorods (the inset is the SAED pattern of the rod) and (d) an HRTEM image of CdS/ZnO nanorods.

For the nucleation and growth of the CdS layer on the ZnO surfaces, the ZnO nanorod array films were immersed in an aqueous solution of $\text{Cd}(\text{NO}_3)_2$ and thioacetamide (TAA; 1:1 molar ratio). The reaction was performed at 80 °C for 8 h to ensure that the surfaces of the ZnO nanorods were covered

fully with CdS. Representative SEM images (Figure S3) of the top and cross-sectional views of the sample indicate that the ZnO nanorod arrays were covered fully with CdS after the deposition process. The experimental results reveal that different concentrations of precursors for the formation of the CdS layer yield different thicknesses of the CdS layer. Thus, if the concentration of precursors increases, the thickness of the CdS layer increases. For an equimolar precursor concentration of 0.024 M, all the surfaces of the nanorods are covered with a thick CdS layer, which is a bulk-like film. At an equimolar precursor concentration of 0.012 M, characterization by high-resolution transmission electron microscopy (HRTEM; Figure 1d) reveals that the thickness of the CdS layer is approximately between 10–15 nm. The lattice fringe of the CdS layer is not clear, which indicates that the crystallinity of the CdS layer after the deposition reaction is quite low. This is consistent with the XRD pattern of the CdS/ZnO nanorod array film characterized and shown in Figure 2a. Accordingly, the CdS diffraction peaks are

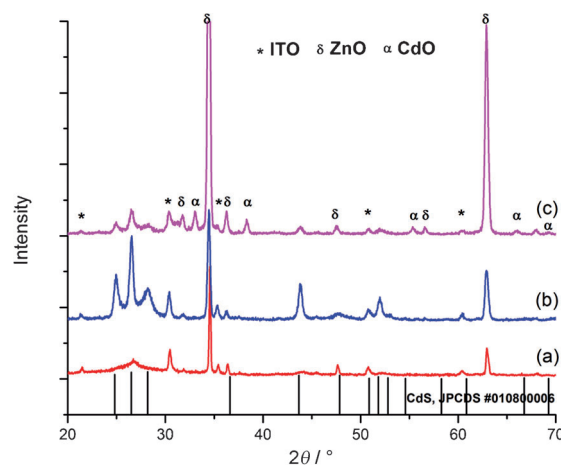


Figure 2. XRD patterns of CdS/ZnO nanorod array films annealed at 500 °C in Ar and air. (a) CdS/ZnO without annealing, (b) CdS/ZnO annealed in Ar, (c) CdS/ZnO annealed in air.

broad and quite low in intensity. Representative SEM images of the top view of the ZnO nanorod array film and CdS/ZnO nanorod array film are presented in Figure 1a and b, respectively. The chemical compositions of the CdS/ZnO nanorod structures are further confirmed by energy dispersive X-ray (EDX) analysis and EDX elemental mapping techniques (Figure S4). It is clear that the ZnO nanorod was covered fully by the CdS layer.

An examination of the optical properties indicates that the CdS/ZnO nanorod arrays can absorb visible light and that the absorption range increased to 560 nm, whereas the bare ZnO nanorod arrays only absorb in the UV region. The absorption edge is also broadened to the red spectral region as the concentrations of the precursors for CdS deposition increased (Figure S5). As reported previously,^[8] the deposition of a CdS coating onto the ZnO nanorod arrays shifts the absorption edge to the visible-light region and promotes the conversion of incident photons into charge carriers (electrons and holes) in the

structures efficiently. Additionally, charge transfer between the CdS and ZnO semiconductors is attributed to the different energy levels of the valence bands and conduction bands; this charge transportation suppresses electron–hole recombination and increases photocatalytic activity significantly. Although a thick CdS layer absorbs light in the visible range efficiently, this layer is less efficient for electron transfer than a thinner layer. We believe that the aggregation of a large number of CdS nanoparticles leads to the formation of many defects in the layer so that these defects might trap the electrons and holes.

The CdS/ZnO nanorod array films were annealed under an air flow to obtain a CdO layer. The annealing temperature was maintained at 500 °C for 1 h. From our experimental observations, the heating rate must be lower than 50 °C h⁻¹ to maintain the stability of the film. For comparison, the CdS/ZnO film was also annealed at 500 °C for 1 h under an inert environment of Ar. The XRD patterns of the samples are presented in Figure 2. Notably, the CdS/ZnO film annealed under Ar has no CdO diffraction peaks (Figure 2b), whereas that annealed under air does (Figure 2c). The CdO diffraction peaks of the CdS/ZnO film appeared after annealing under an air flow prove that a CdO phase exists in the structure by a transformation from CdS. The formation of the CdO layer after annealing in air could follow a solid-state process [Eq. (1)]:



Therefore, annealing without O₂ under Ar cannot form the CdO phase in the film structure. Although the annealing time was prolonged up to 2 h under Ar, no CdO diffraction peaks are observed (Figure S6). The variation in annealing temperature with several CdS/ZnO nanorod array films was performed to reveal the formation process of the CdO phase in the film structure. The XRD patterns of the CdS/ZnO films after annealing at various temperatures for 1 h in air are shown in Figure 3. At the annealing temperature of 400 °C, the CdO phase is still not formed clearly in the structure. However, from 450 °C, the CdO diffraction peaks begin to appear clearly, and the intensity of the peaks increases as the temperature increases. Accordingly, the intensity of the diffraction peaks of the CdS component also decrease as the temperature increases, which shows that the CdS layer has probably

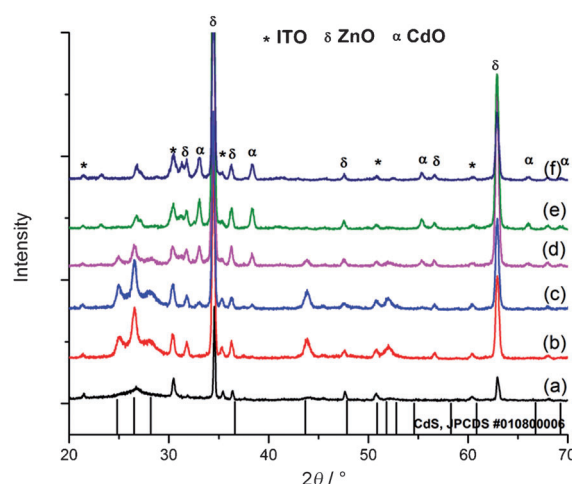


Figure 3. XRD patterns of CdS/ZnO nanorod arrays annealed in air at different temperatures for 1 h. (a) CdS/ZnO without annealing, (b) CdS/ZnO annealed at 400 °C, (c) CdS/ZnO annealed at 450 °C, (d) CdS/ZnO annealed at 450 °C, (e) CdS/ZnO annealed at 550 °C, (f) CdS/ZnO annealed at 600 °C.

been transformed partially on the outer layer surface region. The XRD patterns of the samples annealed at 550 and 600 °C show a few impurity peaks at 2θ = 24 and 32°. The sample annealed at 500 °C was chosen for further investigation.

X-ray photoelectron spectroscopy (XPS) characterization of the CdS/ZnO nanorod film before and after annealing under air at 500 °C for 1 h are shown in Figure 4a, b, and c for the

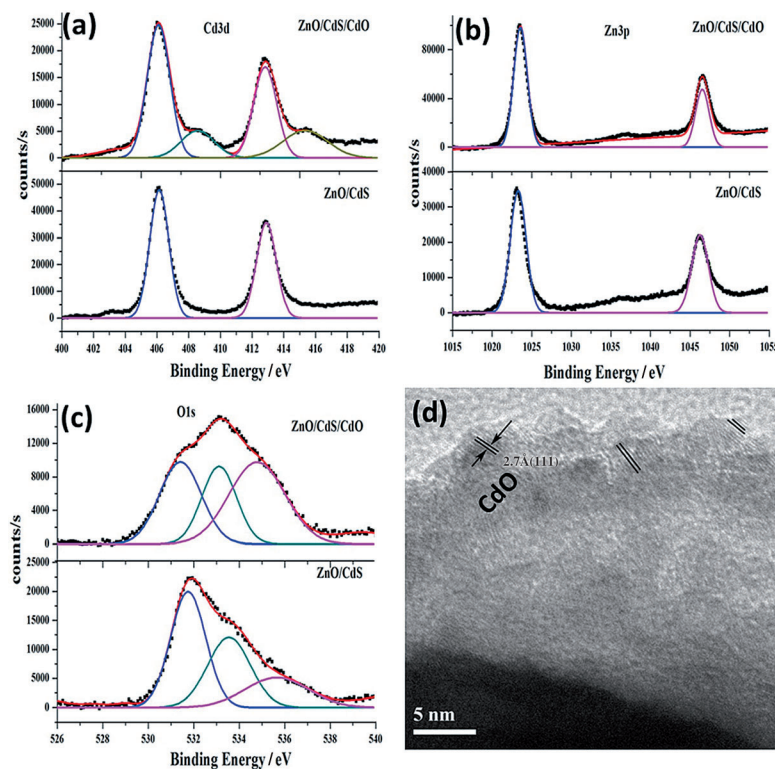


Figure 4. (a–c) XPS spectra of the CdS/ZnO nanorod arrays before and after calcination. d) HRTEM image of CdO/CdS/ZnO.

Cd3d, Zn3p, and O1s peaks, respectively. As presented in Figure 4a, there is a difference between the sample before and after annealing. Before annealing, two peaks at binding energies (BEs) of 406.1 and 412.9 eV are attributed to the bands of Cd3d in the CdS layer. After annealing, in addition to the two existing peaks, there are two other peaks at BE = 408.6 and 415.3 eV, which are attributed to the bands of Cd3d in the CdO layer.^[9] These results confirm that the BE of the Cd–O bond is higher than that of the Cd–S bond. However, it is difficult to distinguish the difference between the BEs of the Cd–O and Zn–O bonds.^[9] Thus, there is no significant change in the XPS peak of O1s. The broader peak in the sample after annealing reveals the increased number of O atoms in the CdO/CdS/ZnO structure.^[10] The annealing process does not affect the structure of the ZnO nanorod arrays inside the CdS layer. Therefore, there is no change in the XPS peaks of Zn3p for the sample before and after annealing. A representative HRTEM analysis of the CdO/CdS/ZnO nanorod sample is presented in Figures 4d and S11 (in higher resolution). The thickness of the CdO layer is estimated to be approximately 5–10 nm. Clear lattice fringes are observed with an interplanar distance of around of 2.7 Å, which is correlated with the (111) facet of CdO formed as an outer layer of the CdS/ZnO rod.

Electrical measurements of the films were also performed to gain further insight into the formation of CdO on the system. CdO is a TCO material that has a high conductivity.^[11] A probe station technique was used to measure the current (*I*) versus potential (*V*) of the films. Figure 5a, b, and c shows the charac-

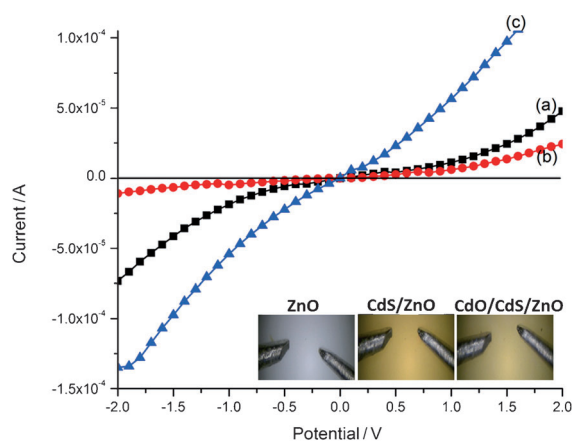


Figure 5. Room temperature *I*–*V* curves of the nanorod array films with probes in contact with the surface of the films. (a) CdS/ZnO film, (b) ZnO film, and (c) CdO/CdS/ZnO film. The insets are optical microscopic images that show the tungsten probes in contact with the films.

teristic *I*–*V* curves at room temperature of CdS/ZnO, ZnO, and CdO/CdS/ZnO nanorod array films, respectively. The insets in the panel are optical microscope images of the films in contact with the tungsten probes. The current of the CdS/ZnO sample is lower than that of the ZnO layer, which is consistent with the typical high conductivity of ZnO. The conductivity of the CdS/ZnO sample annealed at 500 °C for 1 h in air is increased

drastically compared with the others. This again confirms that CdO layers are the outer layer of the nanorod arrays.

All photoelectrochemical properties were measured by using a three-electrode system with 0.35 M Na₂S and 0.25 M Na₂SO₃ as the sacrificial electrolytes, Pt as the counter electrode, Ag/AgCl as the reference electrode, and the photoanode film sample as the working electrode. The photocurrent density of the film samples was evaluated as a function of the applied external potential at a scan rate of 10 mV s⁻¹ under the simulated illumination of 1 sun (100 mW cm⁻²) AM 1.5. The values of the photocurrent density for the CdS/ZnO nanorod arrays reveal the best photoelectrochemical behavior for the photoanode prepared at a precursor concentration of 0.012 M for the deposition of the CdS layer (Figure S7). The photocurrent density increases with the thickness of the deposited CdS layer. However, if the deposited CdS layer is too thick, defects in the aggregated CdS layer trap the photogenerated charge carriers. This trapping of the photogenerated charge carriers might result in the drastic decrease in the photocurrent density (Figure S7 e). For comparison, to take into account the photoelectrochemical performance of the CdS/ZnO films annealed in air, Ar, without annealing, or only bare ZnO nanorod arrays, the photocurrent density of these films was measured. The *I*–*V* curves for the samples prepared under different conditions are shown in Figure 6 (left panel). The dark current is negligible compared to the current under illumination because the dark scan from –1.2 to 1.0 V exhibits a small current density in the range of 10⁻² mA cm⁻². The photocurrent density of the CdS/ZnO nanorod array film is approximately six times greater (≈3.5 mA cm⁻², curve b) than that of bare ZnO (≈0.6 mA cm⁻², curve a) at 0.0 V. Generally, this result under the same conditions is comparable to studies published recently.^[12,13] Compared to that of the CdS/ZnO film, the photocurrent density of the CdO/CdS/ZnO nanorod array film is enhanced significantly (≈4.1 mA cm⁻² at 0.0 V, curve d). Notably, the curve for the CdS/ZnO nanorod array film annealed in Ar is slightly lower than that for the pristine CdS/ZnO nanorod array film, which indicates that the annealing process in an O₂-free environment does not change the crystal structure of the sample.^[14] Furthermore, the slight decrease in the photocurrent density for the sample annealed in Ar could be caused by the increase of the electrical resistivity of the ITO film treated at high temperature.^[15] This result supports our claim that the formation of the CdO layer after annealing the CdS/ZnO nanorod arrays in air enhances the photoelectrochemical properties of the structure. *I*–*t* curves of the samples at 0.0 V were measured to study the photoresponse of these structures over time. The photoresponse of the samples was observed under light illumination (Figure 6, right panel). As the excitation causes a transient effect, the photocurrent returns quickly to a steady state. This result confirms that the charge transfer occurs quickly from layer to layer and can be switched reproducibly from the “ON” to “OFF” state through illumination by light. The CdO/CdS/ZnO nanorod arrays exhibit photocatalytic properties for H₂ evolution at 0.0 V, and the films are stable under the experimental conditions. If the annealing times were further prolonged for the transformation from the CdS/ZnO nanorod structure to the

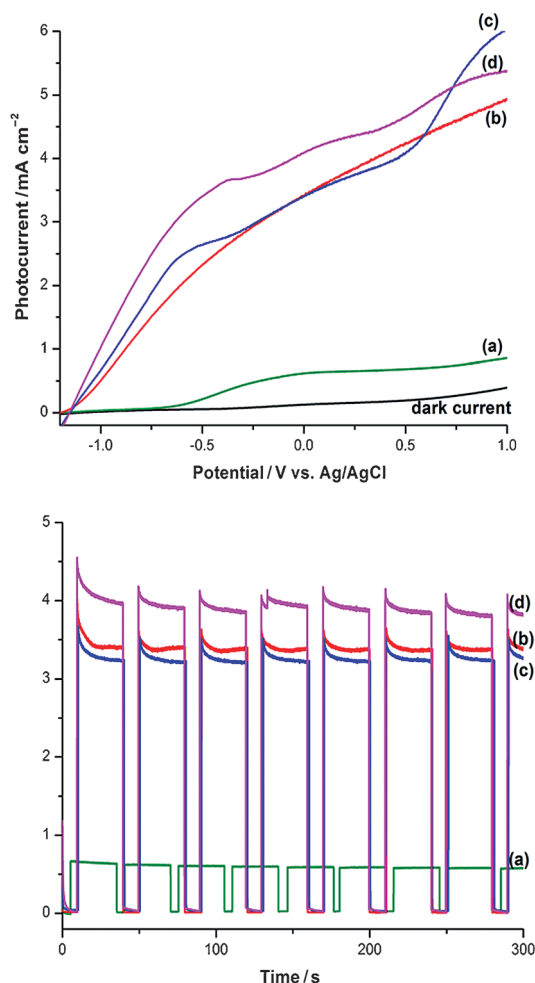


Figure 6. *I*-*V* curves and photoresponse at 0.0 V (Ag/AgCl) for (a) bare ZnO nanorod arrays, (b) CdS/ZnO nanorod arrays, (c) CdS/ZnO nanorod arrays calcined in Ar, and (d) CdO/CdS/ZnO nanorod arrays.

CdO/CdS/ZnO nanorod structure, we observed that the nanorod arrays became aggregated and that the deposited layers became somewhat detached from the structure as the time increased (Figure S8). Accordingly, the photocurrent density decreases with increasing annealing time (Figure S8d). As the annealing time increased, the electrical resistivity of the film increased accordingly,^[15] and the film structure was likely destroyed, which could result in the decrease of the photoelectrochemical behavior.

To evaluate the beneficial effects of the formed CdO layer on the film structure, the incident photon to conversion efficiencies (IPCEs), measured from the short circuit photocurrent density, I_{sc} monitored at various excitation wavelengths at 0.0 V vs. Ag/AgCl, are presented in Figure 7. The IPCE plot of the bare ZnO nanorod arrays shows a peak at approximately 380 nm. This is ascribed to the absorption of ZnO in the solar UV region. The strong response of the IPCE plot was broadened into the visible-light region for the CdS/ZnO and CdO/CdS/ZnO films, which indicates that the CdS and CdS/CdO, respectively, component layers enhance the quantum efficiency. The enhancement of the photocatalytic activity of the hetero-

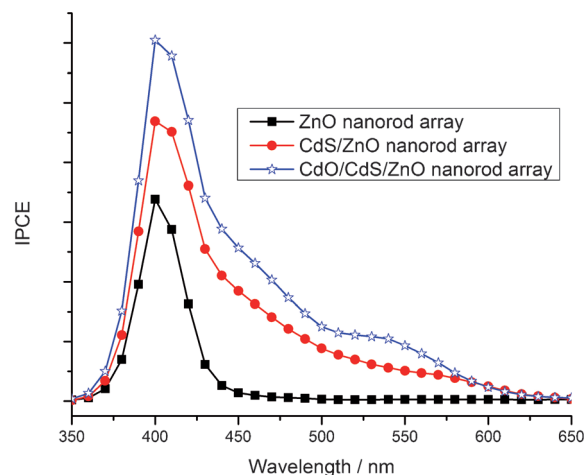
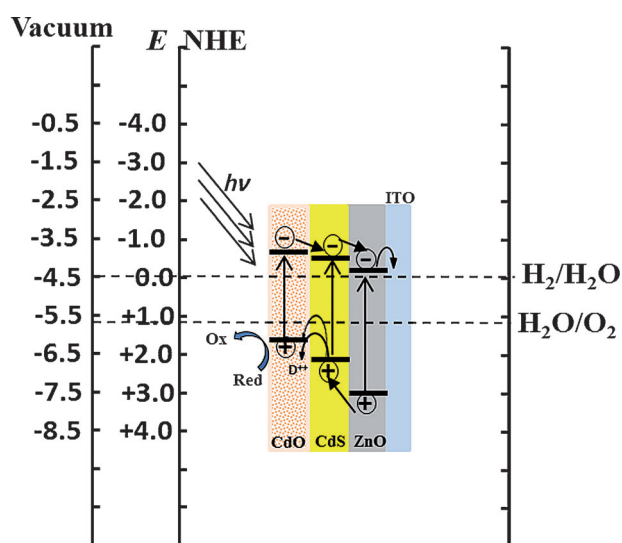


Figure 7. IPCE values measured as a function of wavelength for the films at an external potential of 0 V vs. Ag/AgCl.

structured CdS/ZnO nanorod arrays was explained well by previous studies.^[12] The reasons are the visible-light absorption and the higher charge separation for electrons and holes in the heterostructure. Although many researchers have studied three-component heterostructured photocatalysts, which are considered to be better than two-component photocatalysts, to the best of our knowledge, there is no report on a CdO/CdS/ZnO nanorod array system to date. CdO is a semiconductor with a low band gap of 2.27 eV. The valence band position (O2p) of CdO is found between -8.0 and -3.8 eV.^[7] However, different to the bulk material,^[16,17] from the literature,^[18,19] the band edges of the CdO/CdS/ZnO heterostructure are rearranged as a cascade band structure because of a process known as Fermi level alignment (Scheme 1).^[18] Ultraviolet photoelectron spectroscopy (UPS) analysis of ZnO, ZnO/CdS, and ZnO/CdS/CdO nanorod array films performed using He(I) (21.22 eV) as a photon source are shown in Figure S9. We ob-



Scheme 1. A proposed band-edge diagram for the CdO/CdS/ZnO heterostructured nanorod array.

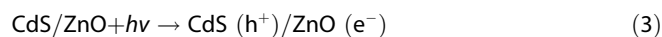
served that the valence band of the ZnO nanoarray film shifts toward negative potentials if it is composited with CdS and CdO, respectively. This is synonymous with a shift of the heterostructure conduction band to more negative potentials. The UPS study has revealed the rearrangement in the heterojunction band structure of the semiconductors. Moreover, a shift of the CdO conduction band toward negative potentials if the CdO/CdS/ZnO electrode is in contact with a redox electrolyte species S^{2-}/S_x^{-2} .^[19] Consequently, the photogenerated charge carriers would be separated readily and transferred efficiently.^[20] However, another possible reason for the enhanced photocatalytic activity is the conductive behavior of the CdO layer, which can separate the holes generated from the CdS. As we mentioned above, CdO is a TCO that has a high conductivity. Many studies on different CdO specimens have shown that CdO always contains a stoichiometric excess of Cd and that the principal point defects are Cd interstitials or oxygen vacancies.^[21] These defects act as charge carriers and result in the high hole mobility and high conductivity of the CdO layer.^[22] This result indicates that the CdO layer can transfer holes from the CdS layer to itself and can reduce electron–hole recombination in the CdS/ZnO nanorod arrays; the reduced recombination enhances the photocurrent density. The proposed mechanism for hole transfer by the CdO layer can be described as follows:

Major defect reaction in CdO [Eq. (2)].^[23]



in which D^{++} is either a doubly ionized oxygen vacancy or Cd interstitial.

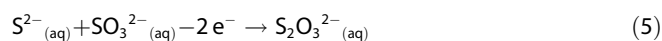
Photocatalytic process [Eq. (3)]:



Hole-transfer process [Eq. (4)]:



Migration^[24] of D^{++} to the electrolyte–semiconductor interface [Eqs. (5) and (6)]:



To investigate the efficient photogenerated charge carrier separations, we performed time-resolved photoluminescence (PL) measurements of the film samples with an excitation laser source of 375 nm and detection wavelength 600 nm. The normalized time-resolved PL decays of ZnO, ZnO/CdS, ZnO/CdS/CdO, and ZnO/CdS film annealed in Ar are presented in Figure 8. Interestingly, the charge lifetime of the ZnO/CdS/CdO nanorod array film is increased drastically compared to that of the others. In particular, the charge lifetime of the ZnO/CdS/CdO film is approximately 93.05 ns, which is much higher than that of ZnO (≈ 19.64 ns) and CdS/ZnO (≈ 27.55 ns). The ZnO/

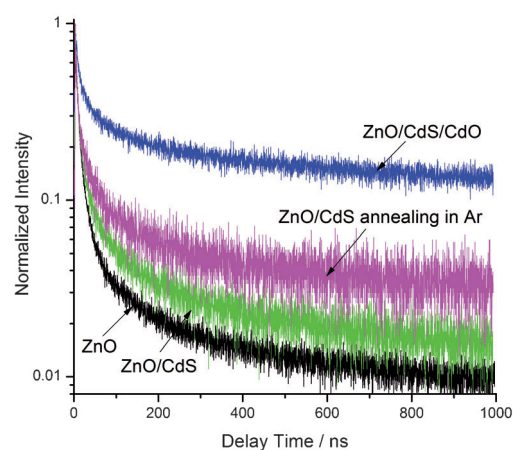


Figure 8. Time-resolved PL decay of the ZnO, ZnO/CdS, ZnO/CdS/CdO, and ZnO/CdS films annealed in Ar.

CdS sample annealed in Ar (an environment that lacks O_2 so no CdO layer is formed) at 500°C for 1 h also exhibits a charge lifetime of approximately 36.88 ns, which is lower than that of the ZnO/CdS/CdO film (i.e., ZnO/CdS annealed in air at 500°C for 1 h). The lifetime of the ZnO/CdS film annealed in Ar is higher than that of the ZnO/CdS film without annealing because of its increased crystallinity. The XRD patterns presented in Figure 2 confirm the crystallinity of the films. This confirms that a thin CdO layer on the ZnO/CdS nanorod arrays can retard the recombination of the photogenerated e^-/h^+ pairs in the ZnO/CdS structure. Consequently, the photoelectrochemical performance of the ZnO/CdS nanorod array electrode can be enhanced by a composited CdO layer.

We also investigated the photoelectrochemical properties of the samples in an electrolytic solution of 0.25 M Na_2SO_4 without using sacrificial agents to study the protection effect of the CdO layers. As we hypothesized, the CdO layer prevented contact between the electrolyte and the CdS layer. Therefore, CdO baffled the photocorrosion of the CdS layer. The I – V curves shown in Figure S10 (left) illustrate the increase in the onset potential (at -0.5 V) compared with the onset potential with sacrificial agents presented above (-1.2 V). Additionally, the photocurrent density (1.2 mA cm^{-2} at 0 V) is much lower than that if sacrificial agents are used. This result could be understood by the difference in the pH values of the Na_2SO_4 electrolyte solution (pH 7) and the electrolyte solution with the sacrificial agent (pH 11); sacrificial agents also play a role as photogenerated-hole scavengers that suppress the recombination of photogenerated holes and electrons.^[25] As shown by the photoresponse presented in Figure S10 (right), the photocurrent density of the CdS/ZnO nanorod array film in the electrolytic solution without a sacrificial agent decreases drastically to 0.4 mA cm^{-2} (close to the curve for bare ZnO) after only one illumination cycle, whereas the value for the CdO/CdS/ZnO nanorod array films decreased slowly. Notably, the CdO layer somehow protects the CdS layer partially. However, the CdO layer is a porous layer, so the electrolyte can permeate through. Thus, the CdO layer cannot protect the CdS layer completely.

Conclusions

Our results demonstrate that an outer CdO layer that surrounds the CdS/ZnO nanorod arrays is formed after an annealing process under air. The CdO/CdS/ZnO heterostructured nanorod array electrode can enhance the photoelectrochemical performance of the device significantly. Proposed mechanisms for photogenerated charge carrier separation in the system were discussed in detail to explain the enhancement of the photocatalytic activity of the electrode. Moreover, the CdO layer somehow offers partial protection against the well-known photocorrosion of the CdS/ZnO system by preventing direct contact between CdS/ZnO and the electrolyte. However, the CdO layer is porous, so the electrolyte can permeate through. Thus, the CdO layer cannot protect the system completely. The simple CdO/CdS/ZnO system can be further applied to enhance the efficiency of the water splitting reaction for hydrogen evolution or for solar cell devices.

Experimental Section

Materials

Zinc acetate (Zn(ac)₂, Aldrich 98%), diethanol amine (Aldrich 99%), ethanol (Aldrich, 99.9%), mucasol (Merz), zinc nitrate hydrate (Zn(NO₃)₂, Aldrich 99.999%), hexamethylenetetramine (HA, Aldrich 99.5%), cadmium nitrate (Cd(NO₃)₂, Junsei 98%), and thioacetamide (TAA, Junsei 98%) were used without further purification. Glass coated with indium tin oxide (ITO) was cleaned by sonication in 3% mucasol solution (once) and in distilled deionized water (DDW; three times) for 30 min.

Growth of ZnO nanorods

A solution of Zn(ac)₂ (2.5×10^{-3} M) in ethanol (50 mL) with diethanol amine (1 drop, 13 mg) was stirred at 60 °C for 1 h. Then, ITO-coated glass was spin-coated with the prepared solution three times. The coated ITO glass was calcined at 500 °C for 30 min to obtain the ZnO seed layer. Equimolar solutions of Zn(NO₃)₂ and HA were prepared at different concentrations. An ITO-coated glass with the ZnO seed layer was immersed in the prepared solution (50 mL) and tilted at 45° in the autoclave. Hydrothermal treatment was performed at 60 °C for 2 h, 70 °C for 2 h, 80 °C for 2 h, and finally at 90 °C for 2 h. The ZnO nanorod array film was rinsed several times with copious amounts of DDW to remove all residues.

Deposition of CdS layer on the ZnO nanorod arrays

Equimolar solutions of Cd(NO₃)₂ and TAA were prepared at different concentrations. A ZnO nanorod array film was immersed in the prepared solution (50 mL) and was tilted at 45° in the autoclave. Then, the reactant solution was kept in the oven at 80 °C for 8 h. The CdS/ZnO nanorod array film was rinsed several times with copious amounts of DDW to remove all residues.

Preparation of CdO/CdS/ZnO nanorod arrays

The CdS/ZnO nanorod array film was annealed under an air flow at 500 °C for 1 h. To maintain the stability of the film, the heating rate was set at 50 °C h⁻¹. At heating rates higher than 50 °C h⁻¹, the

films were scratched or destroyed during the subsequent process to measure the photocurrent.

Photocurrent measurements

The photoelectrochemical properties of the film electrodes (diameter = 1.3 cm) were measured by using a PL-9 Potentiostat/Galvanostat. A three-electrode cell was used that contained a solution of 0.35 M Na₂S (Aldrich, 98%) and 0.25 M Na₂SO₃ (Aldrich 98%) as electrolytes with Ag/AgCl in saturated KCl as a reference electrode, a Pt wire as a counter electrode, and the film as a working electrode. The external electrical voltage was applied from -1.3 to +1.0 V at a scan rate of 10 mV s⁻¹. *I*-*V* curves were obtained in the dark or under illumination. The chronoamperometry curves were measured at 0.0 V. The samples were illuminated with simulated sunlight from a 300 W Xenon lamp (Asahi Spectra HAL-320, ozone free) with a HAL AM 1.5 G filter with an intensity of 1 sun (100 mW cm⁻², corrected spectrally) in front of the sample surface. IPCEs were derived from Equation (7):

$$\text{IPCE} = (I_{sc} [\text{mA cm}^{-2}] \times 1240 [\text{W nm A}^{-1}]) / (P_{\text{light}} [\text{mW cm}^{-2}] \times \lambda [\text{nm}]) \quad (7)$$

in which I_{sc} is the photocurrent density, P is the intensity of monochromatic light, and λ is the wavelength of monochromatic light.

Characterization

SEM images of films were obtained by using a field-emission scanning electron microscope (Hitachi S-4300). The TEM images, SAED patterns, and chemical compositions were obtained by using a JEOL transmission electron microscope (JEM 2100F) with an EDX analyzer at an acceleration of 200 keV. A small amount of the powdered sample was dispersed in ethanol (99.9%), and a drop of the mixture was placed on a carbon-coated microscopic copper grid (300 mesh). The XRD patterns of the samples were recorded with CuK_α radiation ($\lambda = 1.54056 \text{ \AA}$) by using a Rigaku X-ray diffractometer at 40 kV and 150 mA with a scanning rate of 0.02° per step over a range of $10^\circ \leq 2\theta \leq 90^\circ$. Diffuse reflectance UV/Vis spectra of the samples were acquired by using a Varian Cary 5000 UV/Vis-NIR spectrophotometer equipped with an integrating sphere. The surface states of sample were analyzed by XPS (SIGMA PROBE, ThermoVG, UK). The XPS spectra were acquired by using a monochromatic AlK_α photon source at 15 kV and 15 mA. The BEs of the peaks were calibrated relative to the C 1s peak at BE = 286.14 eV. UPS measurements were conducted at the Korea Basic Science Institute (KBSI) by using an AXIS Ultra DLD instrument (KRATOS Inc.) using a He I UV source (21.2 eV) and recorded with a constant pass energy of 5 eV in the ultrahigh vacuum chamber. Time-resolved PL charge lifetime measurements were conducted by using a Micro Time-200 (PicoQuant, Germany) with an excitation laser source of 375 nm and a detection wavelength of 600 nm. Topographic AFM images were recorded at RT by using a Nanoscope III (Digital Instrument) in contact mode with a silicon nitride tip. The *I*-*V* characteristics of the films were measured by using a Keithley model 420-SCS semiconductor characterization system at RT, which can source DC voltage and measure current. The tungsten probes were used as electrodes in contact with the surface of the film in at the same relative distance to perform the electrical measurements.

Acknowledgements

This research was supported by the Korea Center for Artificial Photosynthesis (KCAP) located in Sogang University and funded by the Ministry of Science, ICT and Future Planning (MSIP) through the National Research Foundation of Korea (no. 2009-0093885), and the Brain Korea 21 Plus Project in 2014.

Keywords: electrochemistry · cadmium · nanostructures · photochemistry · zinc

- [1] a) X. Wang, C. J. Summers, Z. L. Wang, *Nano Lett.* **2004**, *4*, 423; b) K. Honda, A. Fujishima, *Nature* **1972**, *238*, 37; c) K. Sivula, R. Zboril, F. L. Formal, R. Robert, A. Weidenkaff, J. Tucek, J. Frydrych, M. Grätzel, *J. Am. Chem. Soc.* **2010**, *132*, 7436; d) H. G. Cha, J. Song, H. S. Kim, W. Shin, K. B. Yoon, Y. S. Kang, *Chem. Commun.* **2011**, *47*, 2441; e) T. Tatsuma, S. Saitoh, Y. Ohko, A. Fujishima, *Chem. Mater.* **2001**, *13*, 2838.
- [2] K. Takanezawa, K. Hirota, Q.-S. Wei, K. Tajima, K. Hashimoto, *J. Phys. Chem. C* **2007**, *111*, 7218.
- [3] G. Wang, X. Yang, F. Qian, J. Z. Zhang, Y. Li, *Nano Lett.* **2010**, *10*, 1088.
- [4] X. Wang, G. Liu, G. Q. Lu, H.-M. Cheng, *Int. J. Hydrogen Energy* **2010**, *35*, 8199.
- [5] P. V. Kamat, *Chem. Rev.* **1993**, *93*, 267.
- [6] K. R. Gopidas, M. Bohorquez, P. V. Kamat, *J. Phys. Chem.* **1990**, *94*, 6435.
- [7] a) G. Choudhary, V. Raykar, S. Tiwari, A. Dashora, B. L. Ahuja, *Phys. Status Solidi* **2011**, *248*, 212; b) Y. Yang, S. Jin, J. E. Medvedeva, J. R. Ireland, A. W. Metz, J. Ni, M. C. Hersam, A. J. Freeman, T. J. Marks, *J. Am. Chem. Soc.* **2005**, *127*, 8796.
- [8] D. R. Baker, P. V. Kamat, *Adv. Funct. Mater.* **2009**, *19*, 805.
- [9] B. V. Christ in *Handbook of Monochromatic XPS Spectra: the Elements of Native Oxides*, Wiley, Weinheim, **2010**.
- [10] A. Manekkathodi, M.-Y. Lu, C. W. Wang, L.-J. Chen, *Adv. Mater.* **2010**, *22*, 4059.
- [11] A. J. Varkey, A. F. Fort, *Thin Solid Films* **1994**, *239*, 211.
- [12] Y. Tak, H. Kim, D. Lee, K. Young, *Chem. Commun.* **2008**, 4585.
- [13] T. P. Nguyen, P. L. Rendu, N. N. Dinh, M. Fourmigue, C. Meziere, *Synth. Met.* **2003**, *138*, 229.
- [14] a) Y. Tak, S. J. Hong, J. S. Lee, K. Yong, *Cryst. Growth Des.* **2009**, *9*, 2627; b) P. Wu, H. Zhang, N. Du, L. Ruan, D. Yang, *J. Phys. Chem. C* **2009**, *113*, 8147; c) P. Kundu, P. A. Deshpande, G. Madras, N. Ranvishankar, *J. Mater. Chem.* **2011**, *21*, 4209.
- [15] C. Li, T. Ahmed, M. Ma, T. Edvinsson, J. Zhu, *Appl. Catal. B* **2013**, *138*, 175.
- [16] M. Grätzel, *Nature* **2001**, *414*, 338.
- [17] Y. Xu, M. A. A. Schoonen, *Am. Mineral.* **2000**, *85*, 543.
- [18] Y. L. Lee, Y. S. Lo, *Adv. Funct. Mater.* **2009**, *19*, 604.
- [19] J. H. Bang, P. V. Kamat, *ACS Nano* **2009**, *3*, 1467.
- [20] A. Kudo, Y. Miseki, *Chem. Soc. Rev.* **2009**, *38*, 253.
- [21] M. Yan, M. Lane, C. R. Kannewurf, R. P. H. Chang, *Appl. Phys. Lett.* **2001**, *78*, 2342.
- [22] F. P. Koffyberg, *J. Solid State Chem.* **1970**, *2*, 176.
- [23] A. R. West in *Basic Solid State Chemistry*, Wiley, **1999**, p. 329.
- [24] R. Jin, W. Gao, J. Chen, H. Zeng, F. Zhang, Z. Liu, N. Guan, *J. Photochem. Photobiol. A* **2004**, *162*, 585.
- [25] O. Madelung, U. Rössler, M. Schulz, *Landolt-Börnstein—Group III Condensed Matter – Numerical Data and Functional Relationships in Science and Technology*, Springer, **1999**, 41B.

Received: April 30, 2014

Revised: July 7, 2014

Published online on October 16, 2014